ARMA 13-517

Relationships between slow slip, seismicity and fluids leakage during a pressurized fault zone rupture in situ experiment: Importance for reservoir/caprock stimulation monitoring and efficiency assessment

Guglielmi, Y. and Henry, P.
Aix-Marseille Université, CNRS, IRD, CEREGE, Aix en Provence, France.
Cappa, F. and Derode, B.
University of Nice Sophia-Antipolis, Côte d'Azur Observatory, Geoazur, Sophia-Antipolis, France.

ABSTRACT: We present a field experiment where we nucleated slow slip at 0.28 km depth through the artificial pressurization of a normal fault while continuously monitoring strain, seismicity and pore pressures. The episodicity of fault slip is related to dilatancy-strengthening revealed by transient pore-pressure drops that correspond to both permeability and porosity increase of the fault zone. We calculate that the slip is initiated by the fault material frictional weakening, the pore pressure increase just being the trigger. Then, there is a competition between high pressure fluid diffusion in the fault zone and multiple slow ruptures that generate 80% of the seismic energy released by tremor-like seismic events. We show that the permeability/porosity increase progressively become the predominant control on slip of larger fault segments. We conclude that variations in the pressure transients and tremors are good indicators of the fluids migration and damaging effects in the fault zone. Some of these events may be considered as precursors to the fault slip activation and some attributes of the signals could be inverted to estimate fault zones stability evolution. Such results are of interest for seismologists and reservoir engineers in natural and induced earthquakes and fault leakage prediction and risk assessment.

1. INTRODUCTION

Understanding the evolution of the hydraulic properties during faults zones rupture, and the links with induced seismicity is important in a broad range of applications at the frontiers of geomechanics and geophysics. Indeed, fluid hydromechanical interactions in fault and fracture zones with contrasting properties are critical for the potential of rock failure which, in turn, may provide flow paths for fluid leakage [1–3]. Considering a Mohr-Coulomb behavior, the increases of fluid pressure will lower the effective stress and fault strength, which can lead to seismic ruptures [4]. If the fluid pressure is high enough, it not only facilitates the slip by reducing the normal stress, but may cause hydrofracturing of the intact rock by tensile cracks, interconnecting and branching pre-existing fractures. Although fluid-injection experiments have shown that a change in fluid pressure level can be accompanied by seismic events [5–6], no simple relationship has been established between the injection rates and seismicity [7]. Reasons for the difficulties in developing such relationships are mainly (1) the lack of in situ experiments with simultaneous seismic and fluid-induced-poroelastic deformations monitoring, and (2) the simple Mohr-Coulomb type arguments that can hardly capture complexities of geomechanical nature [8–9]. Consequently, fundamental uncertainties exist as to how fluid pressures induce rupture, to what extent this rupture is seismic and how this in turn controls the evolution of hydraulic response and the variations of permeability.

In this paper, we report measurements of strain, seismicity and fluid pressure that we continuously monitored during an in situ borehole injection experiment where we nucleated slow slip reactivation on a 10-m long segment of a normal fault. Our observations reveal that a temporal evolution of the induced seismicity characterized by the occurrence of tremors may be related to changes in the fault hydromechanical response. We discuss the relationships between fluids pressure diffusion, fault plastic deformations and tremors through a quasi-static fully coupled hydromechanical analysis of fault slip evolution with time.

2. GEOLOGICAL AND EXPERIMENTAL SETTING

We selected a N030-70°W fault with a meter scale offset in the South-East France sedimentary basin (Fig.1a). The fault intersects limestone layers characterized by a porosity of 4-to-10%, a permeability of 1-to-4×$10^{-13}$$m^2$,

and a Bulk modulus of 30-to-40 GPa. The fault is a 2-m thick zone with sub-parallel pre-existing connected fractures of metric scale. Discontinuous thin breccias zones can be observed close to some fracture planes. The fault zone has an average permeability of $10^{-12}m^2$ and a bulk modulus of 10-to-17 GPa that are a factor 25 higher and a factor 2-to-5 lower than the surrounding country rock, respectively [10]. The experiment was set through the fault zone in a vertical well at a depth of 282-m where a 1.5-m long chamber was isolated between two inflatable packers (Fig.1b and c).

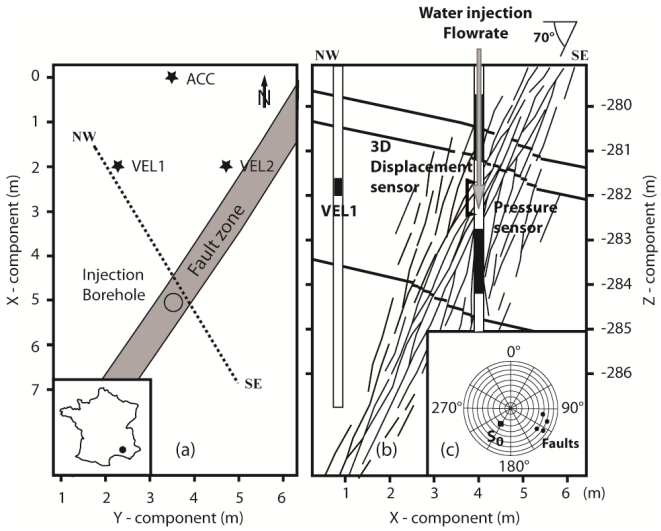

Fig. 1. (a) Map view of the injected fault zone, (b) Vertical cross section with the injection and monitoring devices set across the fault and (c) Stereographic projection of the main fracture planes (upper hemisphere, S_0 is bedding plane pole).

The apparatus necessary for the in situ deformation measurements is a probe (called HPPP probe) that can be lowered in boreholes down to depths of 300 to 500 meters [11]. The HPPP probe allows simultaneous high-frequency sampling of pressures, injection flow rates and 3D deformations of the open hole wall in the 1.5-m long injection chamber, respectively, with sensitivities of 10^3Pa in pressure, 0.1 Liter/min in flow rate and 10^{-6} in deformations. In the probe injection chamber, there is a 3D deformation sensor which is made of an upper and of a lower anchors linked with a deformable metal body. When anchored to the borehole wall with a dedicated hydraulic device, the sensor is free to move from the remaining HPPP probe elements (the two inflatable packers and the down hole injection valve). The metal body deformation is monitored with 20 fiber optic Bragg gratings fixed at different locations on the body. Calibrations in the laboratory allowed reconstructing the metal body 3D deformation from the signals monitored at these 20 fiber optic sensors. When the sensor which can be 0.25-to-0.5m long is anchored across the fault, the deformation of the metal body then captures the 3D relative displacements of the anchors which is induced by the hydromechanical deformation of the fault walls.

In the experiment, deformations were converted into fault tangential and normal displacements measured at a sampling frequency of 1 Hz. Synchronously, the seismic emissions were recorded at 8 kHz by a set of one 3-component accelerometer (ACC, Fig. 1a-b) and two 3-component geophones (VEL1 and VEL2, Fig. 1a) inside boreholes around the injection zone. These three sensors allow for a precise discrimination of seismic events in the near field (2-to-3 meters) of the injection source.

Water was injected at a slow rate for a fixed amount of time. Rate was then increased and again held for the same amount of time. This was repeated for about 30 minutes while monitoring fault slip activation and seismicity.

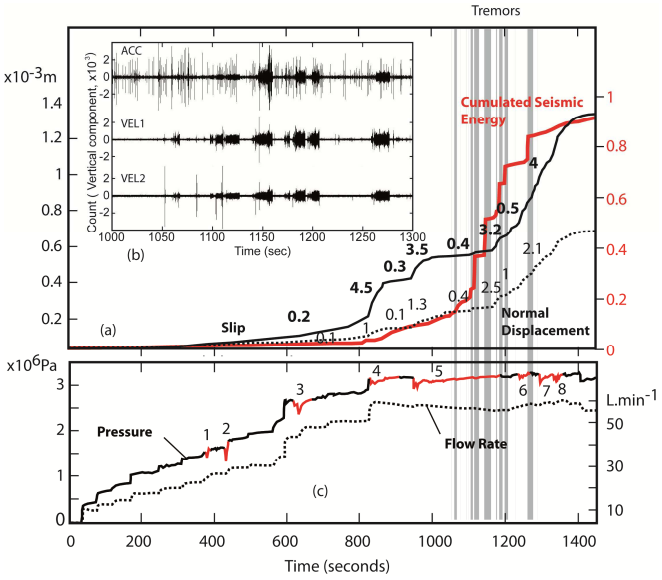

Fig. 2. (a) In situ monitoring of fault slip, normal displacement and cumulated seismic energy (values 0.2-to-4.5 and 0.1-to-2.5 respectively correspond to slip velocities and dilatant rate expressed in micrometers per seconds), (b) Zoom of the Y-component accelerometer signal recorded at ACC in the 1000 to 1400 seconds time interval. This component was chosen because of the high energy radiated by the tremor shear waves in that direction. This curve displays an example of the different seismo-acoustic events recorded during the experiment, (c) Pressure and injected flow rate variations with time (second order pressure drops are numbered from 1 to 8 and figured in red on the pressure curve)

3. IN SITU HYDROMECHANICAL ACTIVATION OF THE FAULT ZONE

Figure 2a shows that the fault slip and normal displacement curves display episodic variations with time characterized by a low amplitude slip that initiates from 0 to 825 seconds, followed by intercalated high and low amplitude slip periods. Low amplitude slip periods velocities and dilation rates progressively increase with time respectively from 0.2-to-0.5 µm.s-1 and 0.1-to-1

μm.s-1 showing an irreversible acceleration of the fault slip nucleation. After 1190 seconds, there is a 50% increase of the dilation rate while slip velocity remains about the same showing that the fault zone becomes more dilatant after that time. At 1375 seconds, there is a return to lower slip rate until the end of the experiment when pressure is shut down at 1450s.

In Fig. 2a, the cumulated seismic energy which was averaged from seismic events energies recorded at the three seismometers (located in Fig. 1) shows that fault movement is mainly seismic between 825 and 1250 seconds. In more details, there is an abrupt increase in the seismic energy from 1100 to 1200 seconds that clearly occurs during a low amplitude slip period to progressively vanish at 1250 seconds when a fault high amplitude slip regime is installed. This energy increase corresponds to a drastic increase in the number of seismic events and to the appearance of low frequency, low amplitude and several seconds long tremor-like events (Fig. 2b). It shows that the 1100-to-1200 seconds seismic period is characterized by the occurrence of many small energy ruptures. To the contrary, the preceding 825-to-1100 second period is characterized by a smaller number of relatively high energy, high-frequency, high-amplitude and short duration events synchronous to two major high amplitude slip events. Thus, at about 1100 seconds, a drastic change in the seismicity occurs with no correlation to slip. These observations are in accordance with slip events triggered by fluid injections in deep wells [9 and 12] where slip measured at the borehole wall after the injection showed values larger than the slip motion associated with seismic events (as evaluated from events magnitudes). In our experiment, the continuous slip monitoring shows that many seismic sources are not located and do not explain all the slip released on the fault segment where the fluid pressurization is occurring. Eventually, we cannot exclude that a part of the observed seismicity may be triggered by slow aseismic slip during the 1100-1200 seconds period.

Figure 2c shows that fluid pressure in the injection chamber displays first order step increase variations that depend on the fault zone diffusivity response to the steps of injected flow rate, and second order variations that correspond to a series of pressure transients. These events display a slight order 0.1-to-0.3MPa instantaneous pressure drop followed by a-several-seconds-long recovery to initial value. Transients 1 and 2 occur at low fluid pressures of 1.7MPa which correspond to the value needed to initiate fault slip. They display a single pressure drop-recovery curve. While fluid pressure increases to a maximum value of 3.5 MPa and fault progressively slips, the pressure transients become more complex. They occur synchronously with high amplitude slip episodes and display multi-pressure drops and recovery curves. One single transient roughly corresponds to a slip of 40×10^{-6} m and a normal displacement of 7×10^{-6} m. If we consider that the stress drop cannot be larger than the maximum initial shear stress of 1.6 MPa and, using Eshelbee [13] equation relating the stress drop on a circular crack to the maximum slip, we get opening fault segments radii around 10×10^{-2} m. In our experiment, the low amplitude slip periods intercalated to the two episodic high amplitude slip events at 825 and 900 seconds and the slowing of the slip after 1375 seconds correlate with pressure transients that appear high enough to depressurize and significantly induce shear strengthening of the fault.

Nevertheless, this shear strengthening effect does not explain the increase in the slip velocities of the low amplitude slip periods, the increase in the dilation rate and the relationships with seismicity observed over the 1400 seconds long experiment (Fig.2a). If we focus on transient 5 that initiates during the large slip event at 900 seconds, the plot in figure 2c shows that although the recovery is fast for a few seconds initially, the pressure drops again with lower amplitudes and does not get back to the pre-slip event value until 1190 seconds when a new high amplitude slip episode initiates. This anomalously long recovery is synchronous with a low amplitude slip period when a factor-of-4 increases in the dilation rate occurs for a slight factor-of-1.2 increase of slip velocity (Fig.2a). Such a slip velocity increase appears insufficient to explain the changes in the fault dilation according to laboratory experiments where factor-of-10 increases in velocities are required to induce significant dilation variations [14]. It means that a significant amount of the dilation released in the injected zone is related to inelastic strain occurring at other locations of this fault zone. The drastic increase in the number of small ruptures and the tremors observed during this 1100-1190 seconds period reflects that slow slip takes place in these zones influencing fault dilation in the injected area.

4. MODELING

We conducted a quasi-static numerical analysis to reconstruct the permeability and friction variations with fluid pressure and slip in the fault zone and to explore the role of fluids in tremor triggering. We considered a heterogeneous fault figured as a 2m thick membrane affected with anisotropic poro-elastic and frictional properties (Fig.3a). Heterogeneities in the fault zone were represented as narrow zones with a dip angle of 70°W divided into 0.2 m thick/0.2 m long solid elements. The evolution of rupture in the modeled fault zone assumed changes in effective stress driven by fluid pressure variations together with the strength variation of the fault heterogeneities.

The commercial finite-difference code FLAC3D [15] was used. A strain-softening hydromechanical model was built following a Coulomb failure criterion with non-zero tension cut-off. Cohesion and friction in the fault zone were assigned to be a function of the plastic component of the total strain. A horizontal-to-vertical stress ratio of 0.5 (i.e. extensional stress regime) was set to the model boundaries in accordance with the regional stress ratio. The in situ flow rate-versus-time experimental curve was imposed at the injection chamber's walls. The calculated pore pressure fields at the end of each pressure step were used for an effective stress (σ_n–P_p) calculation of the elasto-plastic response of the solid. Poro-elastic (effective permeability and storage coefficient) and strength (friction coefficient) rock properties were first dynamically matched to experimental slip curves with an accuracy of 5 x 10^{-6} m (middle graph in Fig.3b). We then explored failure zones propagation with time (upper graph and snapshots in Fig.3b).

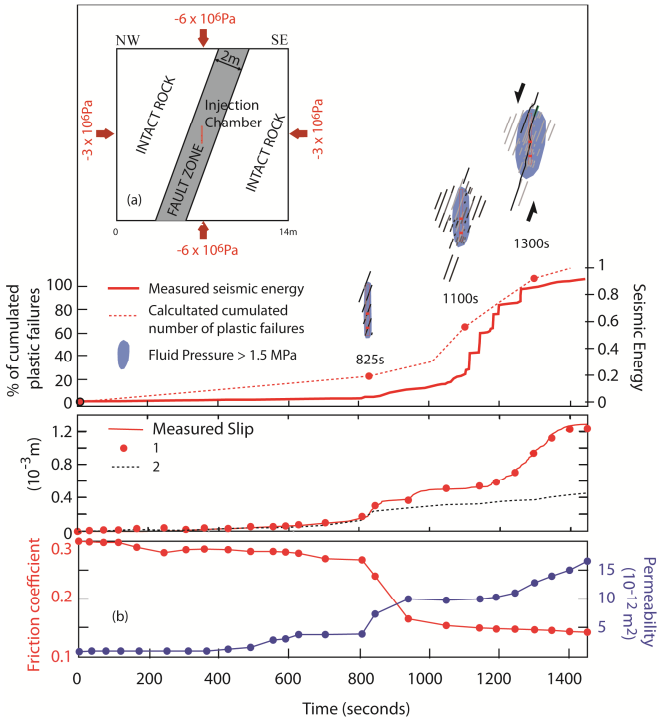

Fig. 3. (a) 2D plane strain numerical fault zone model, (b) Fault permeability and friction variations. In the middle graph, red points illustrate the numerical estimations of fault slip when frictional weakening and permeability variations are allowed, and dashed line when frictional weakening but no permeability variations is allowed.

When fault seismic nucleation occurs at 800 seconds, the striking result of our model is to identify three successive steps of the fluid influence in fault failure, which respectively are stress, strain and permeability (flowrate) dependent. Indeed, from 825 to 950 seconds, fault instability is triggered by the high 2.5 MPa fluid pressure. Snapshot at 825 seconds in Figure 3b shows that failure is characterized by a few pluri-decimeter scale plastic shear zones located at the injection chamber walls. It is associated to 10-to-15 % of the cumulated seismic energy corresponding to high energy events related to the episodic slip accelerations (Fig. 3b upper and middle graphs). During this period, high fluid pressure is only the trigger while a factor-of-3 frictional weakening of fault material explains fault slip (lower graph in Fig.3b). Indeed, we show in Figure 3b middle graph (dashed curve), that if the permeability increase is not considered in the model, it does not affect much the calculated slip. From 950 to 1190 seconds, there is a slight decrease of friction and almost no permeability variation. Nevertheless, in the snapshots of Figure 3b, we show that there is fluids diffusion in the fault zone after the 825-to-950 second permeability increase period. The result is that fluid pressure which is applied to a larger area of the fault causes slight effective normal stress decreases. During this period, fault failure is strain dependent, driven by two competing mechanisms, the effective normal stress variation with fluid diffusion time and many slow small-radiated-energy ruptures (tremors) occurring on a larger fault zone than the injected with fluids one (snapshot at 1100s in Fig.3b). Finally, from 1190 seconds to the end of the experiment, there is a gradual factor-of-1.7 permeability increase while friction coefficient remains close to a residual value of 0.1 (Fig. 3b). During this period, fault failure is controlled by the fault permeability and porosity variations on large active shear zone (snapshot at 1300s in Fig. 3b). Porosity increase is illustrated by the numerous transient pressure drops observed during this period. The high dilation rate favors a drained fault behavior characterized by a stable low-to-aseismic slip regime. Permeability increase, which is deduced from the numerical analysis (Fig.3b lower graph) shows that connection between the pores occurs very fast within the large failure plane. It is figured by the significant 5 Liter/min flow rate increase while there is no pressure variation between 1250 seconds and the end of the experiment (Fig.2c). In the figure 3b middle graph (dashed curve), it clearly appears that if permeability increase is not considered in the model at this time, there is a strong underestimation of the slip.

This experiment injects from a packed-off section of a vertical well intersecting a fault zone, hence the pore pressure field, and therefore the effective stress field are 3D. Yet our 2D model which was set in the plane of maximum shear strain along the fault plane overestimates fault properties variations. Indeed, it was shown in previous analyses of in situ pulses in fractures that plane strain analyses may lead to a factor-of-2 overestimate of the fracture hydraulic and mechanical properties influence on both the stress and pressure fields because they do not consider the radial fluid flow

around the injection hole [16]. This overestimate lies in the range of variation of fault zone properties [10].

5. CONCLUSION

This work highlights how necessary it is to consider not only porosity but also permeability variations during an earthquake nucleation period that can last tens of minutes or more. We point out that the evolution of the ratio between the size of the zones where slow slip is controlled by material weakening and that of the zones invaded by high pressure fluids is a key parameter to characterize seismic nucleation in fault zones. Further on, we show that slip periods may be either seismic or aseismic but they systematically generate pressure drops which characteristics could be used to estimate the scale of the activated heterogeneities in a fault zone and whether or not they contribute to a macro-rupture nucleation. We also show that tremor events are related to the propagation of slow slip on large fault segments preceding high permeability fluid migration. Tracking these low frequency, low amplitude and long duration events may be critical to detect pulses of fluid leakage within reservoir/caprock systems.

REFERENCES

1. Hawkes CD, Mclellan PJ, Bachu S. 2005. Geomechanical factors affecting geological storage of CO2 in depleted oil and gas reservoirs. *J Can Petrol Techno* ; 29:1445-1456.
2. Segall P. 2009. Earthquake and volcano deformation. *Princeton University Press*; pp. 432
3. Gaffet S, Guglielmi Y, Cappa F, Pambrun C, Monfret T, Amitrano D. 2010. Use of the simultaneous seismic, GPS and meteorological monitoring for the characterization of a large unstable mountain slope in the southern French Alps. *Geophys J Int*; 182, 1395-1410. doi: 10.1111/j.1365-246X.2010.04683.x
4. Zoback M,, Harjes HP. 1997. Injection-induced earthquakes and crustal stress at 9 km depth at the KTB deep drilling site, Germany. *J Geophys Res*; 102, 18:477-18:491. doi: 10.1029/96JB02814
5. Fehler M. 1989. Stress control of seismicity patterns observed during hydraulic fracturingexperiments at the Fenton Hill Hot Dry Rock geothermal energy site, New Mexico. *Int J Rock Mech Min Sci and Geomech Abstr*; 26, 211-219. doi: 10.1016/0148-9062(89)91971-2
6. Shapiro SA, Audigane P, Royer JJ. 1999. Large-scale in-situ permeability tensor of rocks from induced seismicity. *Geophys J Int*;137, 207–213. doi: 10.1046/j.1365-246x.1999.00781.x
7. Majer EL, Baria R, Stark M, Oates S, Bommer J, Smith B. 2007. Induced seismicity associated with enhanced geothermal systems. *Geothermics*; 36, 185-222. doi: 10.1016/j.geothermics.2007.03.003
8. Suckale J. 2009. Chapter 2 - Induced seismicity in hydrocarbon fields. *Advances in Geophysics*; 51, 55-106. doi: 10.1016/S0065-2687(09)05107-3.
9. Zoback M., Kohli A., Das I. and McClure M. 2012. The importance of Slow Slip on Faults During Hydraulic Fracturing Stimulation of Shale Gas Reservoirs. *Society of Petroleum Engineer, SPE155476*, The Americas Unconventional Resources Conference, Pittsburgh, Pennsylvania, USA, 5-7 June 2012.
10. Jeanne P., Guglielmi Y. and Cappa F. 2012. Multiscale seismic signature of a small fault zone in a carbonate reservoir: Relationships between VP imaging, fault zone architecture and Cohesion. *Tectonophysics*, 554-557, 185-201.
11. Guglielmi Y., Cappa F., Lançon H., Janowczyk J.B., Rutqvist J., Tsang C.F. and Wang J. 2013. Estimation of permeability, elastic and friction properties of fractured rock masses from in situ hydromechanical testing: the High-frequency Pulse Poroelasticity Protocole (HPPP) testing method. Submitted contribution to the ISRM Commission on Testing Methods, *Int J Rock Mech Min Sci and Geomech Abstr special issue.*
12. Cornet, F.H., Helm, H., Poitrenaud, H. and Etchecopar, A. 1997. Seismic and Aseismic Slips Induced by Large-scale Fluid Injections. *Pure appl. Geophys.*, 150, 0033-4553/97/040563-21.
13. Eshelby, J.D. 1957. The determination of the elastic field of an ellipsoidal inclusion, and related problems. *Proc.R. Soc. Lond. A*, 241, doi:10.1098/rspa.1957.0133.
14. Samuelson, J., Elsworth, D., & Marone, C. 2011. Influence of dilatancy on the frictional constitutive behavior of a saturated fault zone under a variety of drainage conditions. *J.Geophys.Res.*,116, B10406, doi:10.1029/2011JB008556.
15. Itasca, 2009. FLAC3D, Fast Lagrangian Analysis of Continua in 3 Dimensions, Version 4.0, Minneapolis, Minnesota, Itasca Consulting Group.
16. Cappa F., Guglielmi Y., Rutqvist J., Tsang C-F., and Thoraval A., 2006. Hydromechanical modelling of pulse tests that measure fluid pressure and fracture normal displacement at the Coaraze Laboratory site, France. *Int J Rock Mech Min Sci*, 43(7):1062:1082.

ACKNOWLEDGEMENT

This work was funded by the French ANR “Captage de CO_2” through the “HPPP-CO_2” project and by the French PACA county through the “PETRO-PRO” project. The authors would like to thank the International Energy Agency/Geothermal Implementing Agreement and the US Department of Energy for their support of this paper which we trust encourages international cooperation on topics being pursued by Annex VII, Advanced Geothermal Drilling and Logging Technologies.